Acta Crystallographica Section D
Biological Crystallography
ISSN 1399-0047

Structures of the Ca^{2+}-regulated photoprotein obelin Y138F mutant before and after bioluminescence support the catalytic function of a water molecule in the reaction

Pavel V. Natashin,[a,b,c] Wei Ding,[a,d] Elena V. Eremeeva,[b,c] Svetlana V. Markova,[b,c] John Lee,[e] Eugene S. Vysotski[b,c]* and Zhi-Jie Liu[a,f]*

[a]National Laboratory of Biomacromolecules, Institute of Biophysics, Chinese Academy of Sciences, Beijing, People's Republic of China, [b]Photobiology Laboratory, Institute of Biophysics, Russian Academy of Sciences, Siberian Branch, Krasnoyarsk, Russian Federation, [c]Laboratory of Bioluminescence Biotechnology, Chair of Biophysics, Institute of Fundamental Biology and Biotechnology, Siberian Federal University, Russian Federation, [d]Center for Biological Imaging, Institute of Biophysics, Chinese Academy of Sciences, Beijing, People's Republic of China, [e]Department of Biochemistry and Molecular Biology, University of Georgia, Athens, Georgia, USA, and [f]iHuman Institute, ShanghaiTech University, Shanghai, People's Republic of China

Correspondence e-mail: eugene.vysotski@gmail.com, zjliu@ibp.ac.cn

Received 1 October 2013
Accepted 28 November 2013

PDB references:
Y138F obelin, 4mrx; Ca^{2+}-discharged conformational state, 4mry

Ca^{2+}-regulated photoproteins, which are responsible for light emission in a variety of marine coelenterates, are a highly valuable tool for measuring Ca^{2+} inside living cells. All of the photoproteins are a single-chain polypeptide to which a 2-hydroperoxycoelenterazine molecule is tightly but noncovalently bound. Bioluminescence results from the oxidative decarboxylation of 2-hydroperoxycoelenterazine, generating protein-bound coelenteramide in an excited state. Here, the crystal structures of the Y138F obelin mutant before and after bioluminescence are reported at 1.72 and 1.30 Å resolution, respectively. The comparison of the spatial structures of the conformational states of Y138F obelin with those of wild-type obelin gives clear evidence that the substitution of Tyr by Phe does not affect the overall structure of both Y138F obelin and its product following Ca^{2+} discharge compared with the corresponding conformational states of wild-type obelin. Despite the similarity of the overall structures and internal cavities of Y138F and wild-type obelins, there is a substantial difference: in the cavity of Y138F obelin a water molecule corresponding to W_2 in wild-type obelin is not found. However, in Ca^{2+}-discharged Y138F obelin this water molecule now appears in the same location. This finding, together with the observed much slower kinetics of Y138F obelin, clearly supports the hypothesis that the function of a water molecule in this location is to catalyze the 2-hydroperoxycoelenterazine decarboxylation reaction by protonation of a dioxetanone anion before its decomposition into the excited-state product. Although obelin differs from other hydromedusan Ca^{2+}-regulated photoproteins in some of its properties, they are believed to share a common mechanism.

1. Introduction

Calcium ion is a ubiquitous intracellular messenger and carries out this function in many eukaryotic signal transduction pathways. In order to understand the regulation mechanisms of calcium and how disturbances of these mechanisms are associated with disease states, it is necessary to be able to measure calcium inside living cells. Ca^{2+}-regulated photoproteins have been successfully used for this purpose for more than four decades (Alvarez & Montero, 2002; Vysotski *et al.*, 2006; Eglen & Reisine, 2008; Pozzan & Rudolf, 2009; Grienberger & Konnerth, 2012; Roura *et al.*, 2013).

Ca^{2+}-regulated photoproteins are responsible for the light emission of a variety of bioluminescent marine organisms, mostly coelenterates (Morin, 1974). The best known and best studied of these photoproteins are aequorin, first isolated from the jellyfish *Aequorea* (Shimomura *et al.*, 1962), and obelin from the hydroid *Obelia* (Vysotski *et al.*, 2006). All Ca^{2+}-

regulated photoproteins that have been isolated to date consist of a single polypeptide chain with a molecular mass of ∼22 kDa to which a peroxy-substituted coelenterazine, 2-hydroperoxycoelenterazine, is tightly but noncovalently bound. Photoproteins can thus be regarded as luciferases containing a stabilized reaction intermediate (Hastings & Gibson, 1963). Ca^{2+}-free photoproteins emit a very low level of light named 'Ca^{2+}-independent bioluminescence', but the light intensity increases a million-fold or more after addition of calcium (Allen *et al.*, 1977). Bioluminescence results from oxidative decarboxylation of 2-hydroperoxycoelenterazine, generating protein-bound coelenteramide in its S_1 excited state (Shimomura & Johnson, 1972; Cormier *et al.*, 1973). The excited coelenteramide relaxes to its ground state with the production of blue light with spectral maxima around 465–495 nm depending on the source organism (Vysotski & Lee, 2004).

Although Ca^{2+}-regulated photoproteins have apparently been detected in many (>25) different coelenterates (Morin, 1974), cloning and sequence analysis have only been achieved for five hydromedusan photoproteins: aequorin (Prasher *et al.*, 1985, 1987; Inouye *et al.*, 1985), clytin (Inouye & Tsuji, 1993; Inouye, 2008; Markova *et al.*, 2010), mitrocomin (Fagan *et al.*, 1993), obelins from *O. longissima* (Illarionov *et al.*, 1992, 1995) and *O. geniculata* (Markova *et al.*, 2002), and light-sensitive photoproteins from the ctenophores *Beroe abyssicola* (Markova *et al.*, 2012), *Mnemiopsis leidyi* (Aghamaali *et al.*, 2011; Schnitzler *et al.*, 2012) and *Bathocyroe fosteri* (Powers *et al.*, 2013). All Ca^{2+}-regulated photoproteins contain three calcium-binding consensus sequences characteristic of EF-hand Ca^{2+}-binding proteins (Tsuji *et al.*, 1995; Vysotski *et al.*, 2006). Apophotoproteins expressed in *Escherichia coli* can be converted into active photoproteins by incubating them with coelenterazine under calcium-free conditions in the presence of O_2 and reducing agents (Shimomura & Johnson, 1975).

The chemistry of the bioluminescent reaction utilizing coelenterazine as a substrate was suggested by McCapra and Chang from a model study of the chemiluminescence of a coelenterazine analogue in an aprotic solvent (McCapra & Chang, 1967). They showed that the oxidative decarboxylation of coelenterazine occurs through several intermediates. The reaction of coelenterazine with oxygen in strongly basic DMSO produces a primary oxygenation product, the C2-peroxycoelenterazine anion, which proceeds to cyclize to a dioxetanone anion. The decomposition of this strained four-membered α-peroxylactone ring leads to generation of the product, an excited-state amide anion. In the case of Ca^{2+}-regulated photoproteins, the active photoprotein formed by the addition of coelenterazine and oxygen to the apophotoprotein is the C2-coelenterazine hydroperoxide, which is most likely to be produced and stabilized with the assistance of residues of the substrate-binding cavity (Eremeeva, Natashin *et al.*, 2013). The hydroperoxide intermediate has now been verified in both chemiluminescence and bioluminescence reactions (Musicki *et al.*, 1986; Teranishi *et al.*, 1994, 1995; Head *et al.*, 2000; Liu *et al.*, 2003; Titushin *et al.*, 2010). Demonstration of the dioxetanone intermediate is more difficult, but there is sufficient indirect evidence from ^{13}C-labelling in the bioluminescence reaction and from a detailed study of the mechanism of the chemiluminescence reaction to assume its existence (Usami & Isobe, 1996).

In strongly basic DMSO, the chemiluminescence reaction has a spectral emission maximum at 455 nm. The amide product is produced in a high yield, and under the same basic conditions the fluorescence spectrum of the

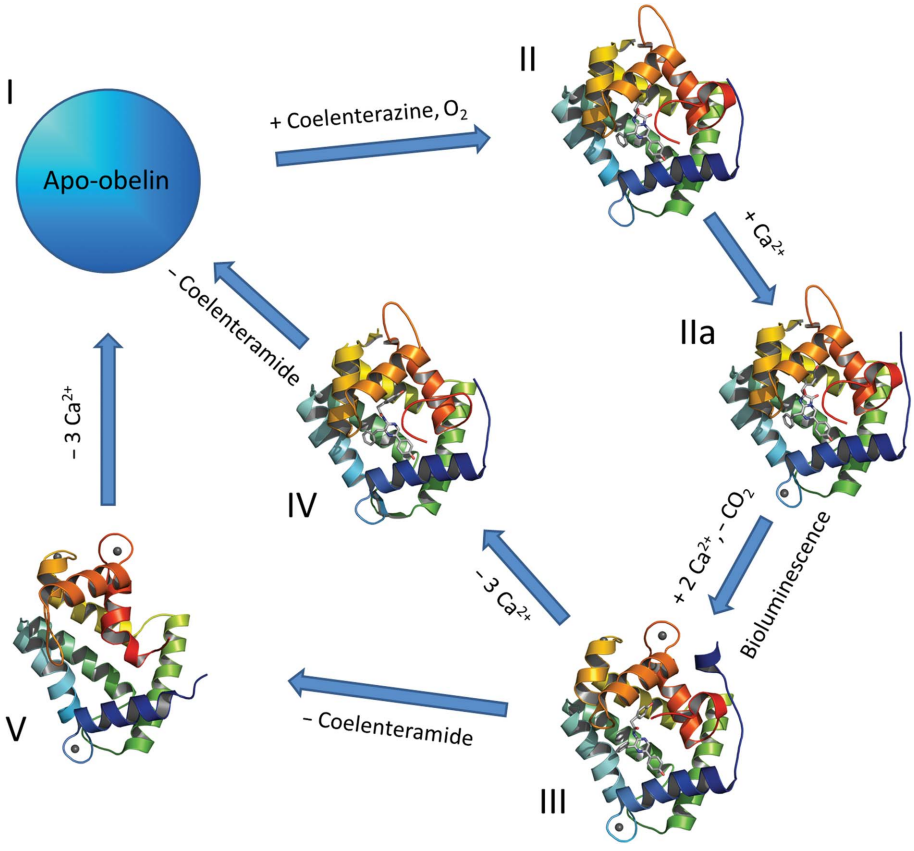

Figure 1
Conformational states of the Ca^{2+}-regulated photoprotein obelin revealed by ^{15}N-HSQC NMR (Lee *et al.*, 2001) and crystallography (Liu *et al.*, 2000, 2003, 2006; Deng *et al.*, 2004, 2005). I, apo-obelin; II, obelin with 2-hydroperoxycoelenterazine (PDB entry 1qv0); IIa, obelin with 2-hydroperoxycoelenterazine and a single Ca^{2+} (PDB entry 1qv1); III, Ca^{2+}-discharged obelin with coelenteramide and three Ca^{2+} (PDB entry 2f8p); IV, Ca^{2+}-discharged obelin with coelenteramide but without Ca^{2+} (PDB entry 1s36); V, apo-obelin with three Ca^{2+} (PDB entry 1sl7). The 2-hydroperoxycoelenterazine and coelenteramide molecules are displayed as stick models in the centre of the protein; the calcium ions are shown as grey balls. The obelin crystal structures are presented in the same orientation.

authentic amide matches the chemiluminescence spectrum. The fluorescing species was identified as the excited amide anion because without added base the fluorescence maximum is at 380 nm from the neutral amide. This model was subsequently extended by a study of the chemiluminescence properties of a number of other coelenterazine analogues (Hori *et al.*, 1973). On the basis of the spectral similarity of this amide-anion fluorescence to the bioluminescence from aequorin, the excited amide anion has been suggested to be the origin of aequorin bioluminescence.

In the past decade, the crystal structures of the photoproteins aequorin (Head *et al.*, 2000), obelin (Liu *et al.*, 2000; Liu *et al.*, 2003) and clytin (Titushin *et al.*, 2010), as well as their ligand-dependent conformational states (Deng *et al.*, 2004, 2005; Liu *et al.*, 2006) (Fig. 1), have been determined. All of these photoproteins and their ligand-dependent conformational states have the same compact and globular structures formed by N- and C-terminal domains, each comprised of two helix–turn–helix motifs known as EF-hands which are characteristic of the EF-hand Ca^{2+}-binding protein superfamily (Vysotski & Lee, 2007). The substrate-binding pocket is highly hydrophobic and is formed by residues originating from each of the helices. In addition, the hydrophilic side chains of two histidine and two tyrosine residues are also directed into the cavity. All of them are found at hydrogen-bonding distances from the atoms of 2-hydroperoxycoelenterazine and have been shown to significantly affect the bioluminescence function of photoproteins (Ohmiya *et al.*, 1992; Ohmiya & Tsuji, 1993; Deng *et al.*, 2001; Vysotski *et al.*, 2003; Malikova *et al.*, 2003; Stepanyuk *et al.*, 2005; Frank *et al.*, 2008; Eremeeva, Markova, Frank *et al.*, 2013; Eremeeva, Markova, van Berkel *et al.*, 2013; Eremeeva, Natashin *et al.*, 2013).

In obelin (Liu *et al.*, 2000, 2003), Tyr138 [equivalent to Tyr132 in aequorin (Head *et al.*, 2000) and Tyr141 in clytin (Titushin *et al.*, 2010)] is hydrogen-bonded to N1 of 2-hydroperoxycoelenterazine. In addition, the hydroxyl group of this Tyr is at a hydrogen-bonding distance from a water molecule which also is hydrogen-bonded to the N atom of the His64 imidazole ring (His58 in aequorin and His67 in clytin). However, in Ca^{2+}-discharged obelin (Liu *et al.*, 2006; the structure of this conformational state is not yet available for other Ca^{2+}-regulated photoproteins), Tyr138 is moved out of the cavity to become solvent-exposed. In the place of Tyr138, a water molecule is found at a hydrogen-bonding distance from this same N atom, now the amide N atom of coelenteramide. Based on these structural findings and studies of the chemiluminescence of a coelenterazine model compound in a protic solvent (Usami & Isobe, 1996), it was assumed that a function of this water molecule is to catalyze the decarboxylation reaction by protonating the dioxetanone anion, which then yields the neutral coelenteramide as the primary excited product in bioluminescence (Liu *et al.*, 2006; Vysotski & Lee, 2007). This hypothesis allowed the rationalization of many of the spectral properties peculiar to coelenterazine bioluminescence *in vitro*.

In the present study, we report the crystal structures of the Y138F obelin mutant before (state II) and after (state III) bioluminescence determined at 1.72 and 1.30 Å resolution, respectively, as well as its spectral and kinetic properties. Our results clearly support a catalytic function of a substrate-binding cavity water molecule in obelin and most likely in the bioluminescence reaction of all Ca^{2+}-regulated photoproteins.

2. Materials and methods

2.1. Preparation of the photoprotein samples

The coding sequence for wild-type (WT) obelin was amplified by PCR using a plasmid with a previously cloned *O. longissima* cDNA gene (Markova *et al.*, 2001) with the following specific primers containing *Nco*I/*Bam*HI sites (lowercase letters) for cloning: forward 5′-ACTccatggCTT-CAAAATACGCAGTTA-3′ and reverse 5′-TTCggatccTTA-GGGAACTCCGTTGCCAT-3′. In addition, for convenience of cloning and because of the insignificance of the N-terminus in the bioluminescence function of photoproteins, Ser2 was substituted by Ala. The PCR product was digested with *Nco*I and *Bam*HI and inserted in-frame into the *Nco*I/*Bam*HI sites of the expression vector pET-19b (Novagen). The resulting plasmid was named pET-19-OL. The Y138F obelin mutant was obtained by mutagenesis with the pET-19-OL plasmid as a template using the QuikChange site-directed mutagenesis kit (Stratagene). The forward 5′-CGAATGGAAAGCTTTG-GAAAAATCTCTG-3′ and complementary reverse primers for mutagenesis were designed according to the manufacturer's protocol. The presence of the Y138F mutation was verified by sequencing.

For apophotoprotein production, transformed *Escherichia coli* BL21-Gold cells were cultivated with vigorous shaking at 37°C in LB medium containing ampicillin. Induction was initiated with 1 m*M* IPTG when the culture reached an OD_{590} of 0.6–0.8. After addition of IPTG, cultivation of the cells was continued for 3 h. The WT obelin and its mutant were purified and activated with coelenterazine (Prolume, Pinetop, USA) as described elsewhere (Vysotski *et al.*, 1999, 2001; Illarionov *et al.*, 2000). The purified photoproteins were homogeneous according to SDS–PAGE.

2.2. Bioluminescence assay

The bioluminescence was measured using a Mithras LB 940 microplate luminometer (Berthold, Germany) by the injection of 50 µl 100 m*M* $CaCl_2$, 100 m*M* Tris–HCl pH 8.8 into a well containing 100 µl 5 m*M* EDTA, 100 m*M* Tris–HCl pH 8.8 and the photoprotein aliquot. The bioluminescence signal was integrated during 6 s.

2.3. Spectral measurements

The bioluminescence and fluorescence spectra were measured using a Cary Eclipse spectrofluorimeter (Agilent Technologies, USA). The emission spectra were corrected using the computer program supplied with the instrument. The bioluminescence spectra were measured in 1 m*M* EDTA, 20 m*M* Tris–HCl pH 7.2 and bioluminescence was initiated by injection of $CaCl_2$ solution in 20 m*M* Tris–HCl pH 7.2. The

Table 1
Data-collection and refinement statistics for the Y138F obelin mutant and its Ca^{2+}-discharged conformational state.

Values in parentheses are for the highest resolution shell.

	Y138F obelin	Ca^{2+}-discharged Y138F obelin
Data processing		
Resolution range (Å)	50.00–1.72 (1.78–1.72)	50.00–1.30 (1.32–1.30)
Wavelength (Å)	0.9789	0.9789
Space group	$P4_1$	$P2_12_12_1$
Unit-cell parameters (Å, °)	a = 73.49, b = 73.49, c = 53.74, $\alpha = \beta = \gamma$ = 90.0	a = 43.61, b = 57.11, c = 68.26, $\alpha = \beta = \gamma$ = 90.0
Unique reflections	30654 (3020)	40375 (1295)
Completeness (%)	100 (100)	94.4 (65.5)
Mean $I/\sigma(I)$	20.07 (4.10)	35.55 (5.71)
R_{merge} (%)	6.8 (45.1)	4.4 (20.9)
Multiplicity	7.3 (7.4)	5.9 (2.6)
Refinement		
Resolution range (Å)	37.357–1.718	34.663–1.299
Reflections used (working/free)	30630/1998	40315/2000
R_{work}/R_{free} (%)	14.0/16.9	17.4/19.3
No. of protein atoms	1601	1591
No. of solvent atoms	298	297
No. of ligand atoms	34	34
Mean B (Å^2)	26.40	13.5
R.m.s.d., bond lengths (Å)	0.019	0.007
R.m.s.d., bond angles (°)	1.735	1.139
Ramachandran statistics, residues in (%)		
Preferred regions	97.5	98.1
Allowed regions	2.5	1.9

concentration of free calcium was ∼0.5 µ*M* in order to provide an approximately constant light level during the spectral scan. In cases where a substantial change in bioluminescence intensity took place during the spectral scan, the data points were also corrected for bioluminescence decay. The fluorescence spectra were measured in 1 m*M* $CaCl_2$, 10 m*M* bis-tris pH 7.0.

2.4. Rapid-mixing kinetics measurements

The kinetics of light response after sudden exposure to a saturating Ca^{2+} concentration were examined using an Applied Photophysics SX20 stopped-flow machine (20 µl cell volume, 1.1 ms deadtime). The temperature was controlled using a circulating water bath and was set at 20°C. The syringes contained a protein sample in 1 m*M* EDTA, 20 m*M* Tris–HCl pH 7.2 and 2 m*M* $CaCl_2$, 20 m*M* Tris–HCl pH 7.2, respectively. The solutions were mixed in equal volumes. Rise and decay rate constants were determined separately with the *SigmaPlot* software using averaging of three shots. The rise and decay rate constants were calculated by one- and two-exponential fitting, respectively. The contribution of the k_1 and k_2 decay rate constants was estimated as the relative amplitude calculated from the fitted amplitudes a and b, with their sum normalized to 1.

2.5. Crystallization, data collection, structure solution and crystallographic refinement

For crystallization, the Y138F obelin obtained after ion-exchange chromatography was exchanged into a buffer consisting of 2 m*M* EDTA, 10 m*M* bis-tris pH 6.5 and was concentrated to ∼18 mg ml^{-1} using Millipore centrifuge tubes. Y138F obelin obtained by charging the apoprotein with high-purity coelenterazine (JNC Corporation, Japan) was used in these experiments. To prepare Ca^{2+}-discharged Y138F obelin, a solution of the obelin mutant was diluted in 4 m*M* $CaCl_2$, 10 m*M* bis-tris pH 6.5 at 4°C to a final concentration of ∼1 mg ml^{-1}. During this procedure, a bright greenish bioluminescence was observed. After the bioluminescence had ceased, the initially yellow protein solution was now colourless, indicating that the coelenterazine had been converted into coelenteramide. To test for the presence of bound coelenteramide, the fluorescence of the final product was measured. The Ca^{2+}-discharged protein was then concentrated to ∼12 mg ml^{-1} using Millipore centrifugal tubes.

A Mosquito crystallization robot (TTP LabTech, UK) and commercially available crystallization screening kits were used for screening initial crystallization conditions. The hits were optimized manually using the hanging-drop vapour-diffusion technique. The best condition for crystallization of Y138F obelin was a solution of 2.1 *M* DL-malic acid pH 7.0 (Wizard IV, Emerald BioSystems). Y138F obelin crystals grew as light yellow rod-shaped crystals after 5–7 d at 4°C. It should be noted that Y138F obelin crystals only grew when the drop comprised 2 µl protein solution and 1 µl precipitant solution. The best condition for the crystallization of Ca^{2+}-discharged Y138F obelin was a solution of 0.2 *M* ammonium nitrate, 20% PEG 3350 (PEG/Ion Screen, Hampton Research). The crystal of Ca^{2+}-discharged Y138F obelin grew as a large colourless rod-shaped crystal after one week at 16°C. The drop consisted of 2 µl protein solution and 2 µl precipitant solution. For X-ray diffraction analysis, the crystal was directly picked up from the crystallization drop using a fibre loop and was flash-cooled in liquid nitrogen.

Data were collected on beamline BL17U1 at the Shanghai Synchrotron Radiation Facility, People's Republic of China. Native diffraction data were indexed, integrated and scaled to 1.72 Å resolution for Y138F obelin and 1.30 Å resolution for Ca^{2+}-discharged Y138F obelin (Table 1) using the *HKL*-2000 software suite (Otwinowski & Minor, 1997). Phases for Y138F and Ca^{2+}-discharged Y138F obelin crystals were determined

Table 2
Comparison of the conformational states of Y138F obelin.

Structural parts of the photoprotein	R.m.s.d. values† (Å) Y138F (II) *versus* Y138F (III)	Y138F (II) *versus* WT (II)	Y138F (III) *versus* WT (III)
Overall‡	2.46/3.26	0.30/1.08	1.52/2.62
N-terminal domain§	1.44/2.04	0.30/1.20	0.54/1.70
C-terminal domain§	2.62/3.80	0.24/0.89	1.91/3.20
EF-hand I¶	1.74/2.20	0.23/0.76	0.36/1.24
EF-hand II¶	0.67/1.68	0.22/1.17	0.40/1.54
EF-hand III¶	1.80/3.19	0.19/0.54	1.40/3.48
EF-hand IV¶	1.94/3.72	0.20/1.02	0.57/1.74

† Calculated using *Superpose* from the *CCP*4 suite (Winn *et al.*, 2011). Values are given for main-chain/side-chain atoms. ‡ Residues 7–195 and 9–191 in conformational states II and III, respectively. § N-terminal and C-terminal domains are defined as residues 7–106 and 9–106 in conformational states II and III, respectively. ¶ EF-hands I, II, III and IV are defined as residues 17–54, 58–104, 110–141 and 149–180, respectively.

by molecular replacement with *Phaser* (McCoy *et al.*, 2007) using the structures of WT obelin (PDB entry 1qv0; Liu *et al.*, 2003) and Ca^{2+}-discharged WT obelin (PDB entry 2f8p; Liu *et al.*, 2006) as search models, respectively. The final models were refined with *PHENIX* (Adams *et al.*, 2002, 2010) and *REFMAC*5 (Murshudov *et al.*, 2011). Manual adjustments to the model were performed using *Coot* (Emsley & Cowtan, 2004). Visualization and superposition of the molecular structures were performed using *PyMOL* (DeLano Scientific LLC). The atomic coordinates and structure factors have been deposited in the Protein Data Bank (Berman *et al.*, 2000) as entries 4mrx and 4mry for Y138F obelin and its Ca^{2+}-discharged conformational state, respectively.

3. Results and discussion

3.1. Overall structure

The spatial structures of the Y138F obelin mutant in states II and III retain the same overall scaffold characteristic of the different ligand-dependent conformational states of Ca^{2+}-regulated photoproteins (Head *et al.*, 2000; Liu *et al.*, 2000, 2003, 2006; Deng *et al.*, 2004, 2005), and both structures closely resemble those of the corresponding conformational states of WT obelin (Liu *et al.*, 2003, 2006) (Figs. 2*a* and 2*b*). The final model of Y138F obelin includes 189 of the 195 amino acids (1601 atoms), the 2-hydroperoxycoelenterazine molecule (34 atoms) and 298 solvent molecules. Residues 1–5 are not visible in the electron-density maps, as is frequently observed for the N-terminal residues in the structures of other Ca^{2+}-regulated photoproteins. The r.m.s.d. of main-chain C^{α} atomic positions of Y138F obelin *versus* WT obelin is only 0.30 Å (Table 2). The final model of Ca^{2+}-discharged Y138F obelin includes 187 amino acids (1591 atoms), the coelenteramide molecule (31 atoms), three Ca^{2+} atoms and 297 solvent molecules. Residues 1–8 are not visible in the electron-density maps. The r.m.s.d. of the 183 C^{α} atomic positions of Ca^{2+}-discharged Y138F obelin *versus* the same conformational state of WT obelin is 1.52 Å (Table 2).

The r.m.s.d.s of main-chain and side-chain atoms of Y138F obelin in conformational state II *versus* conformational state III are 2.46 and 3.26 Å, respectively. These values are a little larger than those for comparison of the corresponding states

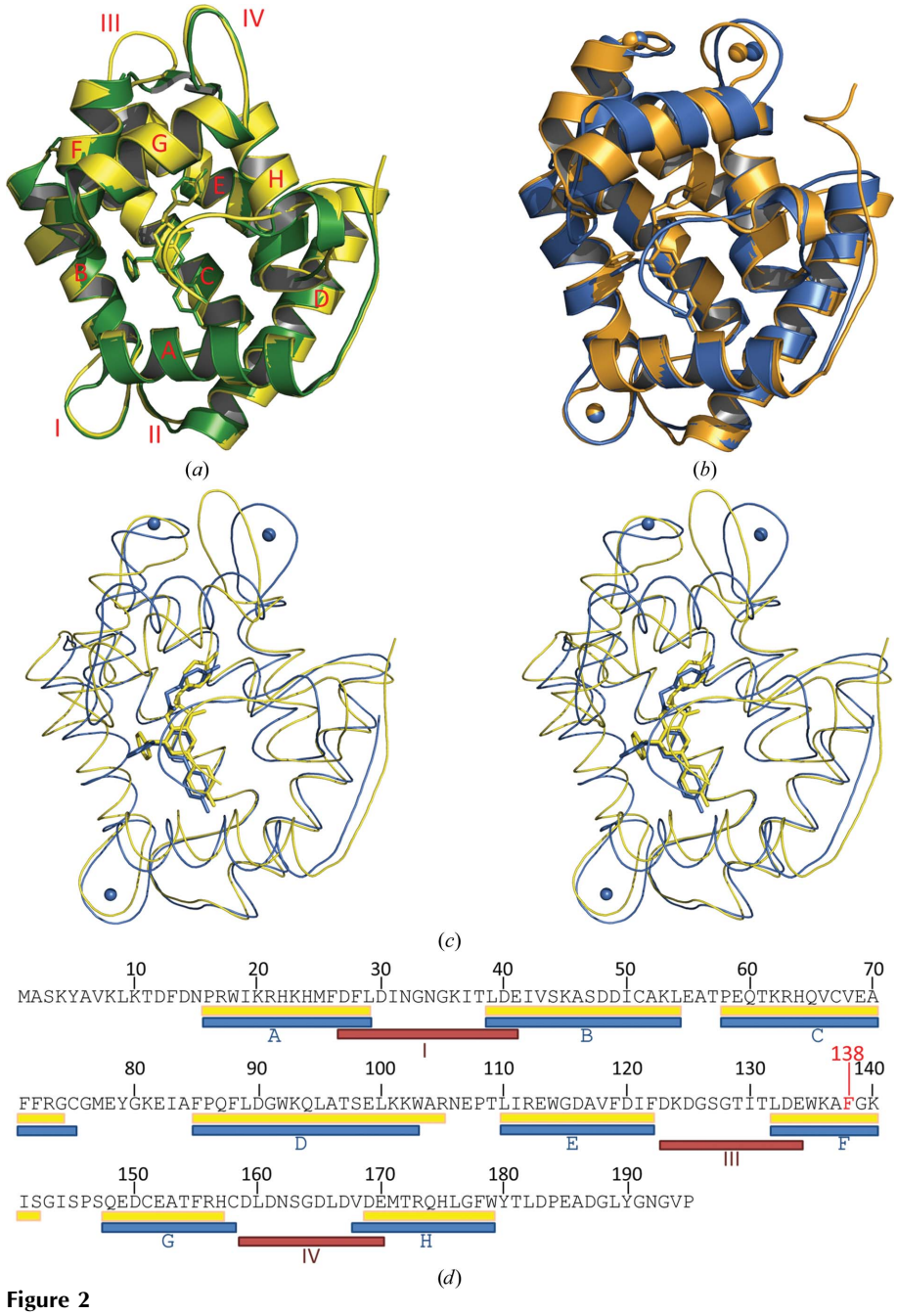

Figure 2
Crystal structures of Y138F obelin in conformational states II and III. (*a*) Superposition of the overall structure of state II of Y138F obelin (yellow) and WT obelin (green). The helices are marked by capital letters A–H. The loops are designated I–IV. (*b*) Superposition of the overall structure of state III Ca^{2+}-discharged Y138F obelin (blue) and WT obelin (brown). All structures are presented in the same orientation. (*c*) Stereoview of the superposition of Y138F obelin II (yellow) and III (blue). The 2-hydroperoxycoelenterazine and coelenteramide molecules are displayed as stick models in the centre of the protein; calcium ions are shown as balls. The 2-hydroperoxycoelenterazine, coelenteramide and calcium ions are coloured according to the structure colour. (*d*) Sequence of obelin from *O. longissima* (Illarionov *et al.*, 1995). The mutation is marked in red. The helices are shown as yellow and blue sticks according to the structures of conformational states II and III of Y138F obelin, respectively. The loops involved in the binding of Ca^{2+} are shown as brown sticks.

of WT obelin (Liu *et al.*, 2006). In spite of this, WT obelin and the Y138F mutant undergo very similar changes in response to Ca^{2+} binding: *i.e.* the C-terminal domain and EF-hand IV alter in conformation more than the N-terminal domain and other EF-hands, while EF-hand II undergoes an insignificant change in both WT and Y138F obelin.

In Ca^{2+}-regulated photoproteins the C-terminus caps the substrate cavity, providing a solvent-inaccessible and nonpolar environment (Head *et al.*, 2000; Liu *et al.*, 2000, 2003; Titushin *et al.*, 2010). This apparently optimizes the efficient population of the first electronic excited state of coelenteramide and favours a high quantum yield for its fluorescence. The inaccessibility of the internal substrate-binding cavity of photoproteins to solvent is the result of hydrogen-bond interactions of helix A residues with residues from helix H and the C-terminus. In Y138F obelin (state II), the $N^{\varepsilon 2}$ atoms of His22 and His24 (helix A) are hydrogen-bonded to the carbonyl O atoms of Trp179 (helix H) and Gly193 (C-terminus), and the $N^{\eta 1}$ and $N^{\eta 2}$ atoms of Arg21 (helix A) are hydrogen-bonded to the carbonyl O atom of Phe178 (helix H), the $O^{\delta 1}$ atom of Asp187 (C-terminus) and the O atom of the C-terminal Pro195. The Ca^{2+}-discharged Y138F obelin (state III) retains these hydrogen bonds and in addition a new one is formed between the $N^{\eta 2}$ atom of Arg17 (helix A) and the $O^{\delta 1}$ atom of Asp187 (C-terminus). This hydrogen-bond pattern exactly corresponds to that found in conformational states II and III of WT obelin (Liu *et al.*, 2000, 2003, 2006).

The structures of all calcium-binding loops and all changes that take place in the calcium-binding loops after reaction in Y138F obelins are essentially the same as in WT obelins (the average r.m.s.d. values of the main-chain atomic positions are ~0.2 Å) and are therefore not shown. In Ca^{2+}-discharged Y138F obelin calcium ions are found in Ca^{2+}-binding sites I, III and IV (Figs. 2*b* and 2*c*). The typical geometrical

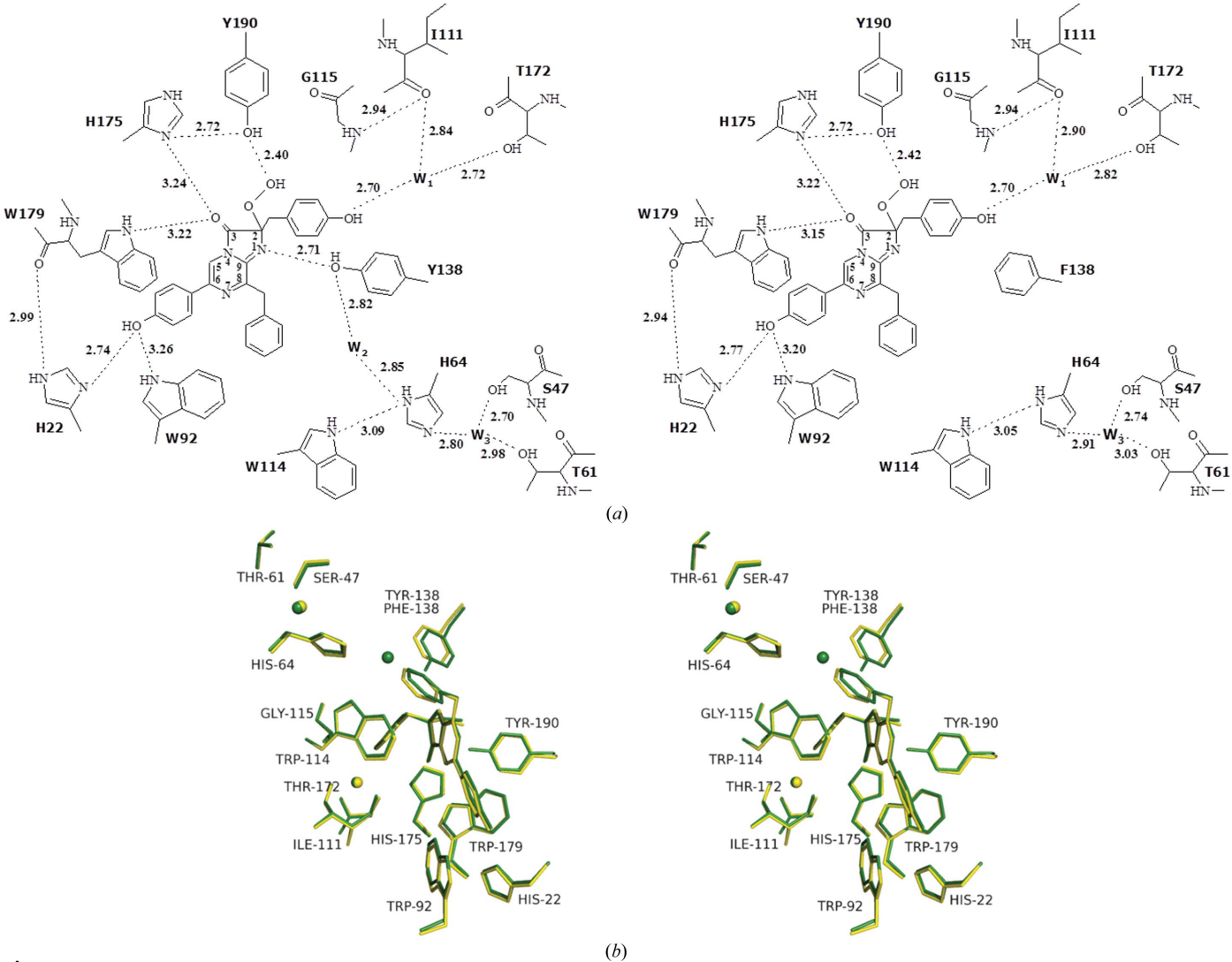

Figure 3
Internal cavities of WT and Y138F obelins. (*a*) Two-dimensional drawing of the hydrogen-bonding network in the binding cavities of WT (left) and Y138F (right) obelins. (*b*) Stereoview of the superposition of 2-hydroperoxycoelenterazine molecules with the key residues facing into the substrate-binding cavities of WT (green) and Y138F (yellow) obelins. Hydrogen bonds are shown as dashed lines. Distances are given in Å. Water molecules are shown as balls coloured according to the structure.

arrangement of O atoms in a pentagonal bipyramid is observed, with the Ca^{2+} occupying the centre of the pyramid. All three Ca^{2+}-binding sites of obelin contribute six oxygen ligands to the metal ion, derived from the carboxylic side groups of Asp and Glu residues, the carbonyl groups of the peptide backbone or the side chain of Asn, and the hydroxyl group of Ser, all with a coordination distance of ∼2.4 Å. The seventh ligand comes from the O atom of a water molecule.

Thus, comparison of the spatial structures of the conformational states of Y138F obelin with each other and with

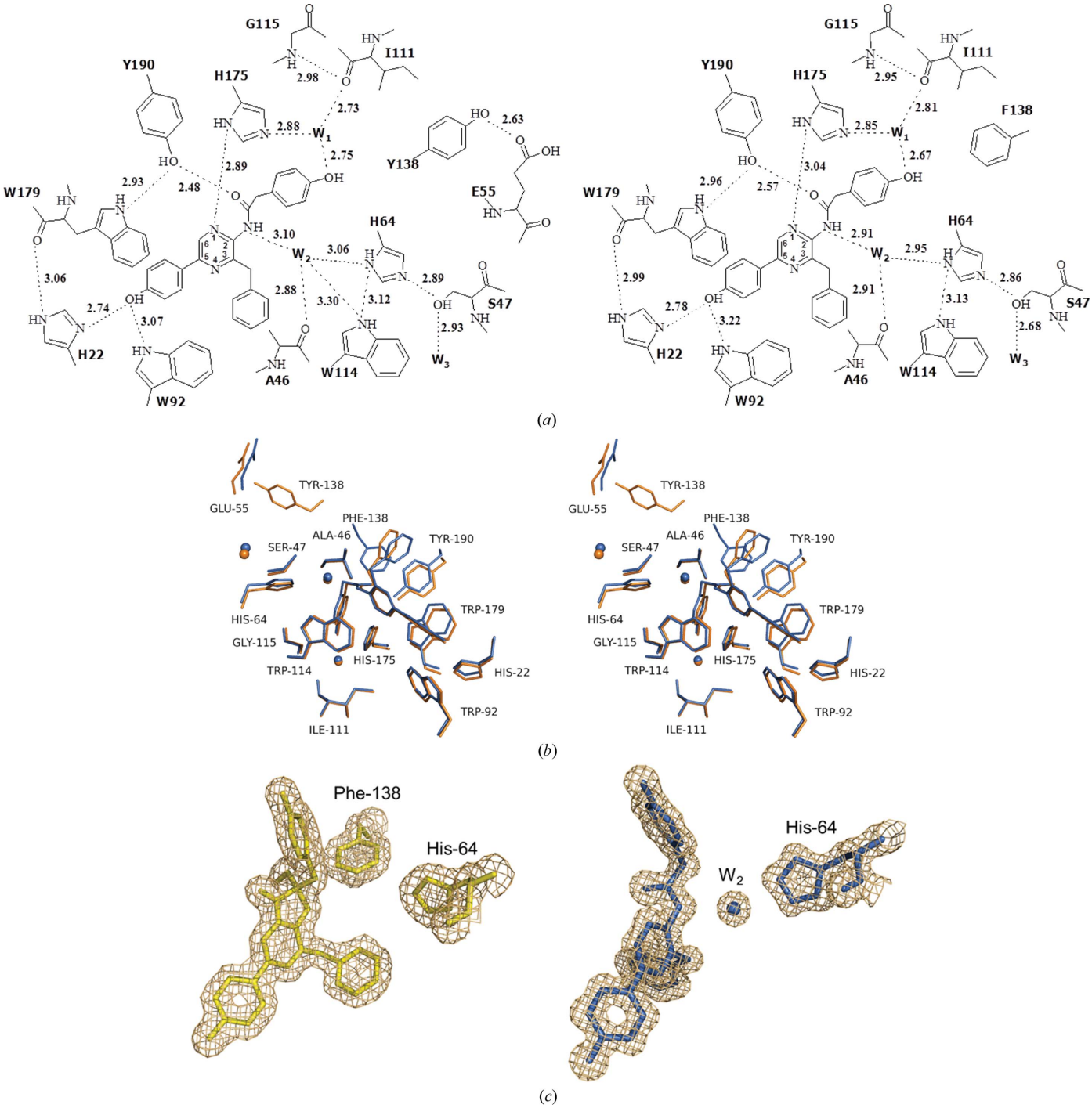

Figure 4
Internal cavities of Ca^{2+}-discharged WT and Y138F obelins. (*a*) Two-dimensional drawing of the hydrogen-bonding network in the binding cavities of Ca^{2+}-discharged WT (left panel) and Y138F (right panel) obelins. (*b*) Stereoview of the superposition of coelenteramide molecules with the key residues facing into the internal cavities of Ca^{2+}-discharged WT (brown) and Y138F (blue) obelins. Hydrogen bonds are shown as dashed lines. Distances are given in Å. Water molecules are shown as balls coloured according to the structure. (*c*) Electron-density maps of 2-hydroperoxycoelenterazine (left) and coelenteramide (right) molecules with some internal cavity residues in Y138F obelin before (state II) and after (state III) the bioluminescence reaction, respectively.

those of WT obelin gives clear evidence that the substitution of Tyr by Phe does not affect the overall structure and structural rearrangements in the obelin molecule in response to calcium binding.

3.2. Structure of the substrate-binding cavity of Y138F obelin before and after the bioluminescence reaction

The residues comprising the binding cavity of Y138F obelin, *i.e.* those within 4 Å of the 2-hydroperoxycoelenterazine, originate from helix A (His22, Met25, Phe28 and Leu29), helix B (Lys45 and Ile50), helix C (Phe72), helix D (Phe88 and Trp92), helix E (Ile111, Trp114, Gly115 and Phe119), helix F (Trp135 and Phe138), the loop linking helices F and G (Ile144), helix H (Met171, His175 and Trp179) and the C-terminus of the protein (Tyr190). They are practically identical to those forming the substrate-binding cavity of WT obelin in the same conformational state (PDB entry 1qv0). There are only two differences: in Y138F obelin, Phe88 of helix A is additionally found within a distance of 4 Å and Ile42 of the helix B shifts further away than 4 Å.

The hydrogen-bonding network for conformational states II of WT and Y138F obelins formed by 2-hydroperoxycoelenterazine and some key residues is shown in Fig. 3(*a*). In WT obelin (state II; Fig. 3*a*, left panel), His22 and Trp92 are at hydrogen-bond distances from the O atom of the 6-(*p*-hydroxyphenyl) group, Tyr190 is hydrogen-bonded to the hydroperoxide group, His175 forms hydrogen bonds to Tyr190 and C3 carbonyl O atom, N^{ε} of Trp179 is hydrogen-bonded to the C3 carbonyl O atom, and the Tyr138 hydroxyl group forms a hydrogen bond to the N1 atom of 2-hydroperoxycoelenterazine. There are also two water molecules W_1 and W_2 which are stabilized by hydrogen bonds to surrounding residues and to the OH of the 2-(*p*-hydroxybenzyl) substituent of coelenterazine. The third water molecule (W_3) is situated close to the surface of the photoprotein molecule and is kept there by hydrogen bonds to His64, Ser47, Thr61 and the main-chain N atom of Gln65 (Fig. 3*a*, left panel). It is noteworthy that the Y138F obelin in conformational state II retains completely the same substrate-binding cavity architecture as WT obelin: all residues are found in practically the same positions (Fig. 3*b*) and the hydrogen-bond distances are essentially the same in both WT and Y138F obelins (Fig. 3*a*, right panel). There is only one substantial difference: the internal cavity of Y138F obelin has no water molecule corresponding to W_2 in WT obelin (Fig. 3*a*, right panel; Fig. 3*b*).

The residues comprising the cavity of Ca^{2+}-discharged Y138F obelin originate from helix A (His22, Met25, Phe28 and Leu29), helix B (Ala46 and Ile50), helix C (Phe72), helix D (Phe88 and Trp92), helix E (Trp114, Gly115 and Val118), helix F (Phe138), the loop linking helices F and G (Ile141), helix H (Met171, His175 and Trp179) and the C-terminus of the protein (Tyr190), *i.e.* essentially the same as in the cavity of state II except for Lys45, Ile111, Phe119, Trp135 and Ile144, which are displaced, and Ala46, Val118 and Ile141, which move into the cavity. It should be also noted that the amino-acid residues forming the cavity of Ca^{2+}-discharged Y138F obelin are almost identical to those comprising the coelenteramide-binding cavity of WT obelin in state III. There are only two differences: in Ca^{2+}-discharged Y138F obelin, Phe138 of helix F, and Ile141 instead of Gly143 from the loop linking helices F and G, are additionally found within the 4 Å cutoff.

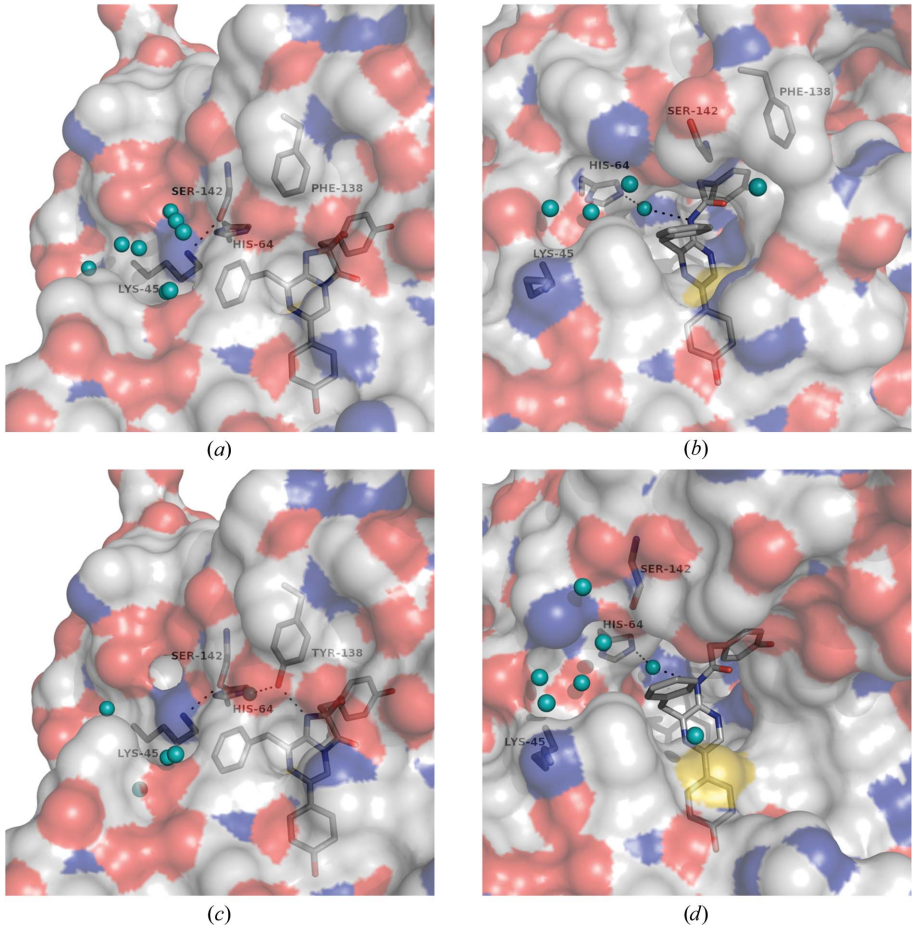

Figure 5
Molecular-surface representation of Y138F and WT obelins in conformational states II and III. (*a*) Y138F obelin (state II). (*b*) Ca^{2+}-discharged Y138F obelin (state III). (*c*) WT obelin (state II). (*d*) Ca^{2+}-discharged WT obelin (state III). A solvent-exposed opening on the surface of Ca^{2+}-discharged Y138F (*b*) and WT (*d*) obelins is shown in the centre. The 2-hydroperoxycoelenterazine, coelenteramide and amino acids are shown as grey stick models. Water molecules are represented as cyan balls. The structures are in the same orientation. Hydrogen bonds are shown as dashed lines. C atoms are shown in light grey; N atoms in blue; O atoms in red and S atoms in yellow.

Fig. 4(*a*) shows a two-dimensional representation of the hydrogen-bonding network in the internal cavities of Ca^{2+}-discharged WT and Y138F obelins formed by coelenteramide and some key residues. In Ca^{2+}-discharged WT obelin (Fig. 4*a*, left panel), the side chains of His22 and Trp92, which were at hydrogen-bonding distances from the O atom of the 6-(*p*-hydroxyphenyl) group of 2-hydroperoxycoelenterazine before reaction (Fig. 3*a*, left panel), are at practically the same distances from the O atom of the 5-(*p*-hydroxyphenyl) substituent of coelenteramide. N^{ε} of Trp179 was hydrogen-bonded to the C3 carbonyl O atom (Fig. 3*a*, left panel), but after reaction this residue forms a new hydrogen bond to Tyr190. Tyr190, which apparently stabilizes the 2-hydroperoxy group of coelenterazine by a hydrogen bond and is also hydrogen-bonded to His175, lacks the hydrogen bond to His175 after the reaction but forms a new hydrogen bond to the carbonyl O atom of coelenteramide. The His175 residue also forms new hydrogen bonds to the N1 atom of coelenteramide and the water molecule W_1, which is repositioned, apparently because of the change in the position of the 2-(*p*-hydroxybenzyl) group of coelenterazine. Owing to repositioning, W1 only retains a hydrogen bond to the carbonyl O atom of Ile111. The hydroxyl group of Tyr138 that originally hydrogen-bonded to the N1 atom now forms a hydrogen bond to Glu55 on the surface of the photoprotein molecule (Fig. 4*a*, left panel). It is apparent that the Tyr138 is replaced by the water molecule (W_2) that connected Tyr138 to His64 in state II (Fig. 3*a*, left panel). As a result, His64 is also slightly shifted toward coelenteramide, retaining the hydrogen bond to W_2. Additionally, W_2 is also now hydrogen-bonded to the carbonyl O atom of Ala46, which appears in the cavity after reaction. Since His64 is shifted, the water molecule W_3 retains a hydrogen bond to Ser47 and forms a new hydrogen bond to the O atoms of Asp48 and Gln65 (Fig. 4*a*, left panel). In the coelenteramide-binding cavity of Ca^{2+}-discharged Y138F obelin all of the residues are found practically in the same positions (Fig. 4*b*) and the hydrogen-bond distances are essentially the same as in Ca^{2+}-discharged WT obelin (Fig. 4*a*, right panel). Some differences are disclosed in the hydrogen bonding of W_3; in the obelin mutant this water molecule is positioned by hydrogen bonds to only Ser47 and Asp48, compared with WT obelin in which the side chain of Gln65 is also involved. In addition, the hydrogen bond between N^{ε} of Trp114 and W_2 disappears in Ca^{2+}-discharged Y138F obelin.

The most remarkable finding was the reappearance of the water molecule (W_2) in the coelenteramide-binding cavity of Ca^{2+}-discharged Y138F obelin (Figs. 4*a* and 4*c*, right panels) since the corresponding water molecule was missing in the structure of state II (Fig. 3*a*, right

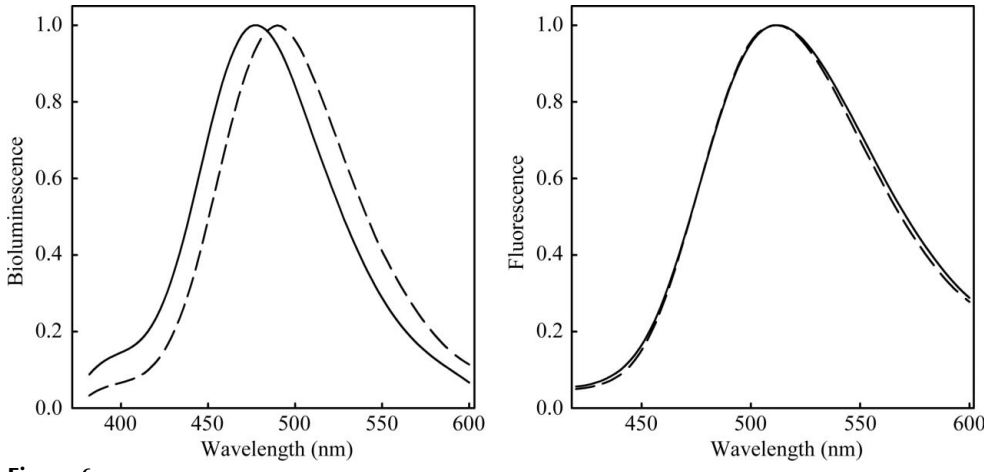

Figure 6
Normalized bioluminescence (left) and fluorescence (right) spectra of WT obelin (solid line) and Y138F obelin (dashed line).

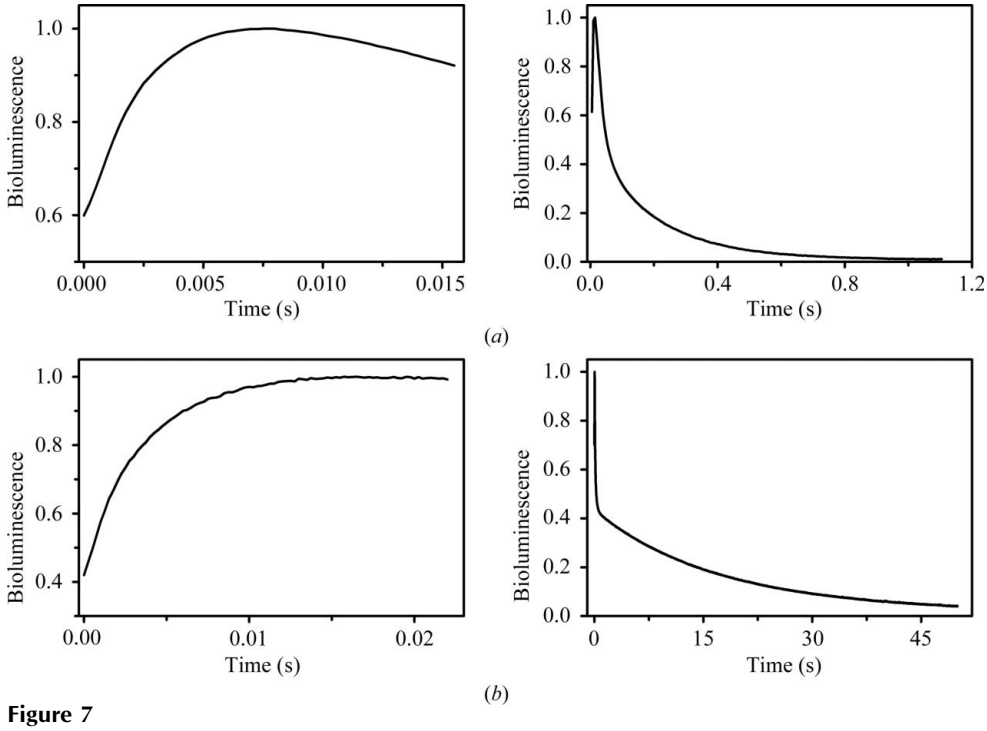

Figure 7
High-speed (left) and low-speed (right) stopped-flow plots of the bioluminescence signals of WT (*a*) and Y138F (*b*) obelins. The protein concentration was 4.5 μ*M* for both proteins. The curves are individual shots.

panel; Fig. 4*c*, left panel). Fig. 5 shows the surface models of Y138F and WT obelins before and after the bioluminescence reaction. Although the changes in the overall structure on Ca^{2+} binding are only 2.46/3.26 Å (Table 2), they are quite sufficient to induce the formation of a solvent-access opening (Fig. 4*b*), which is apparently attributed to repositioning of the Lys45 and Ser142 residues. It should be noted that for Ca^{2+}-discharged WT obelin (PDB entry 2f8p) this 'hole' is also found in the same location on the molecular surface.

3.3. Spectral and kinetic properties of Y138F obelin

In contrast to the substitution of some other residues of the substrate-binding cavity of photoproteins (Ohmiya & Tsuji, 1993; Eremeeva, Markova, Frank *et al.*, 2013), the replacement of Tyr by Phe has no significant effect on the bioluminescence capacity of obelin and its spectral properties; the Y138F obelin preserves 60% of the WT obelin activity and leads to a 10 nm long-wavelength shift of λ_{max} and a decreased shoulder at 400 nm (Table 3; Fig. 6, left panel). However, both obelins in the Ca^{2+}-discharged conformational state III have identical fluorescence spectral distributions with λ_{max} at ~510 nm (Fig. 6, right panel). The differences observed in the bioluminescence spectra of WT and Y138F obelins might be a consequence of small variations in hydrogen-bond distances. This might also affect the efficiency of the excited-state proton transfer from the dissociable 6-(*p*-hydroxyphenyl) group of neutral coelenteramide to His22, resulting in the longer wavelength emission from the coelenterazine phenolate anion (Vysotski & Lee, 2007; Tomilin *et al.*, 2008; van Oort *et al.*, 2009).

However, the bioluminescence kinetics of Y138F obelin are markedly changed compared with WT obelin (Fig. 7). By fitting a single exponential to the rising phase of each light signal (Fig. 7, left panels), we estimated that the rate constant for the rise in bioluminescence decreases from 476.5 ± 1.4 s^{-1} in WT obelin to 305.3 ± 1.4 s^{-1} in Y138F (Table 3), *i.e.* the mutation of Tyr decreases the rate of rise of bioluminescence 1.5-fold compared with WT obelin. The k_{rise} value for WT obelin determined in our experiments is somewhat higher than previously reported (Vysotski *et al.*, 2003), which might be owing to differing experimental conditions or the use of different stopped-flow machines. The decay rate constants of Y138F obelin light emission (Fig. 7, right panel) are also

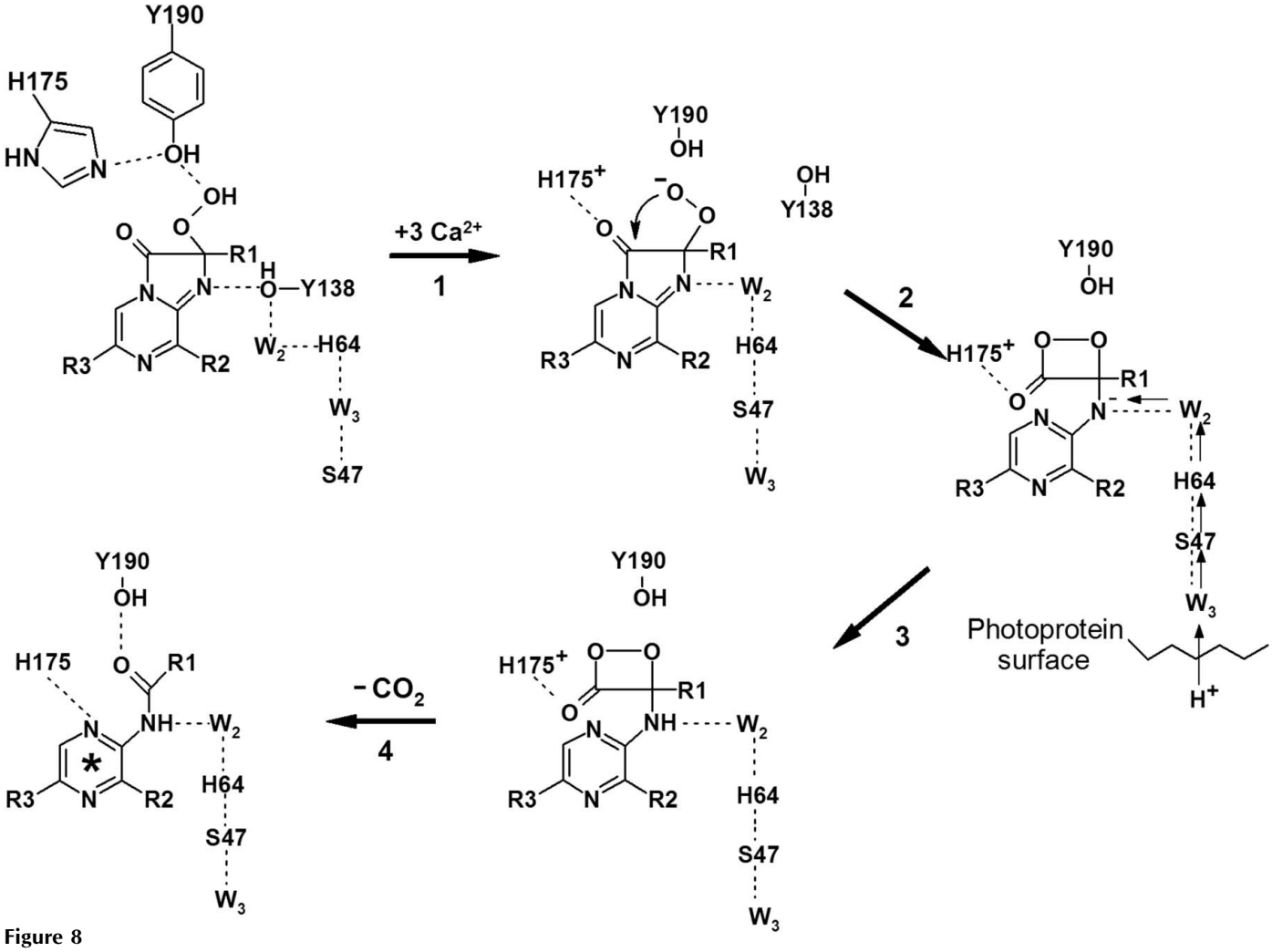

Figure 8
Modified reaction sheme.

decreased: the k_1 and k_2 values for the WT obelin obtained from two-exponential fitting amount to 43.6 ± 0.23 s^{-1} and 5.0 ± 0.01 s^{-1}, respectively, whereas the corresponding constants for the mutant are 13.7 ± 0.3 and 0.06 ± 0.0003 s^{-1} (Table 3). Besides, the mutation increases the contribution of the 'fast' component but decreases the contribution of the 'slow' component in the decay phase.

According to the four-step kinetic model suggested for the bioluminescence reaction of the photoprotein aequorin (Hastings *et al.*, 1969; Blinks *et al.*, 1982), k_{rise} and k_{decay} are attributed to steps corresponding to oxidative decarboxylation of the substrate and conformational rearrangements in the photoprotein molecule as a consequence of Ca^{2+} binding, respectively. Taking into account our kinetic and structural data, we can reasonably conclude that the lack of the water molecule in the internal cavity immediately after Ca^{2+} binding causes the decrease in the rate of rise of bioluminescence in Y138F obelin. Since this water molecule probably appears in the cavity as a result of its diffusion through the solvent-exposed opening (Fig. 5), the bioluminescence reaction takes place although with a slower rate, as the water molecule is almost in position near the amide N atom of coelenteramide in WT obelin, while it has to diffuse into the cavity from the surface in Y138F obelin.

Table 3
Bioluminescent properties of Y138F obelin.

	Bioluminescence				k_{decay}† (s^{-1})	
Obelin	Relative activity (%)	$\lambda_{max}/\lambda_{shoulder}$ (nm)	Fluorescence, λ_{max} (nm)	k_{rise} (s^{-1})	k_1	k_2
WT	100	480/400	512	476.5 ± 1.4	43.6 (0.66) ± 0.23	5.0 (0.34) ± 0.01
Y138F	60‡	490/400	510	305.3 ± 1.4	13.7 (0.8) ± 0.3	0.06 (0.2) ± 0.0003

† The relative contribution of each decay constant is shown in parentheses. ‡ The activity of Y138F obelin is expressed as a percentage of WT obelin activity.

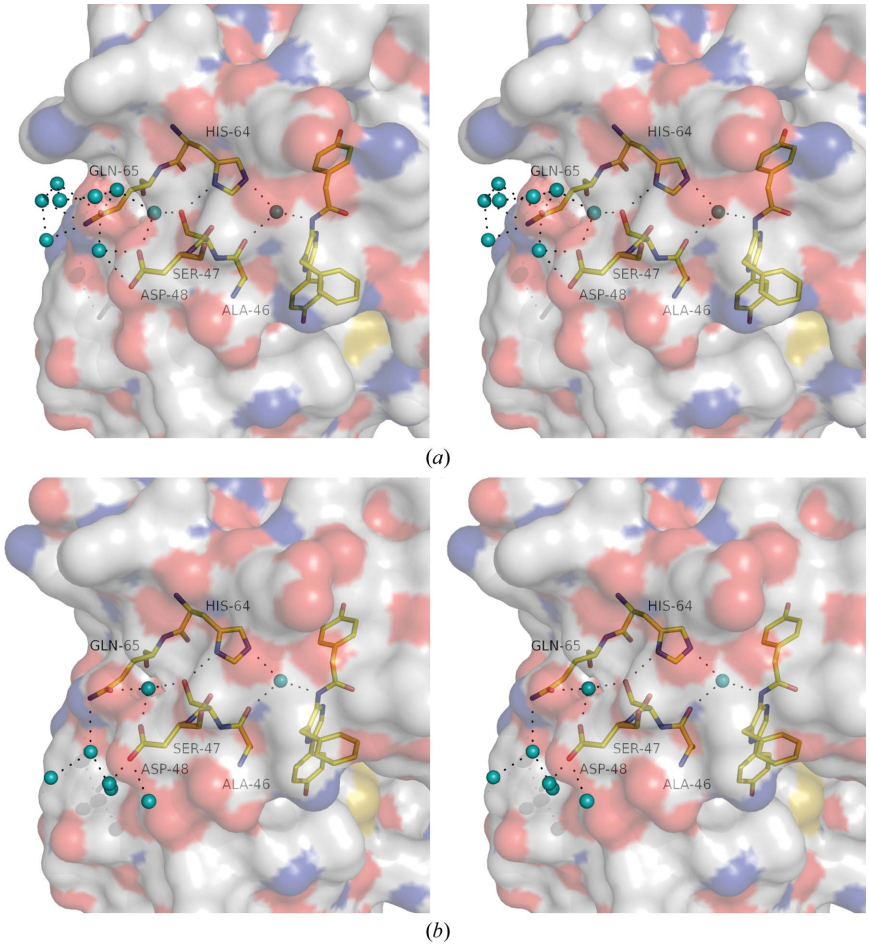

Figure 9
Stereoview of a 'proton channel' in Ca^{2+}-discharged Y138F (*a*) and WT (*b*) obelins. The coelenteramide molecule and amino acids are shown as yellow stick models. Water molecules are represented as cyan balls. Hydrogen bonds are shown as dashed lines. The structures are in the same orientation.

Although in general these results support our hypothesis (Liu *et al.*, 2006; Vysotski & Lee, 2007) that this water molecule catalyzes the decarboxylation reaction of 2-hydroperoxycoelenterazine by protonation of the dioxetanone anion, based on our findings we have slightly modified the reaction scheme (Fig. 8) suggested previously (Liu *et al.*, 2006). It is obvious that the first step in the initiation of photoprotein bioluminescence must be the binding of Ca^{2+} to the loops within the EF-hand motifs. In the family of EF-hand proteins, EF-hand motifs almost always occur in pairs. This double motif appears to be important for correct structural folding and is thought to increase the affinity of each EF-hand Ca^{2+}-binding loop for calcium (Nelson & Chazin, 1998). The paired EF-hands display extensive hydrophobic interactions between the two EF-hand motifs and a short β-type interaction between the two binding loops. The Ca^{2+}-regulated photoproteins are not an exception: in the N-terminal domain EF-hand motif I is paired with EF-hand motif II, which has the characteristic structural features of an EF-hand motif but not the canonical sequence in the loop for calcium binding, and in the C-terminal domain the EF-hand motif III is paired with EF-hand motif IV. The loops of the paired EF-hand motifs show interactions typical of other EF-hand Ca^{2+}-binding proteins by means of hydrogen bonds between main-chain N and carbonyl O atoms (Deng *et al.*, 2005). Among the residues comprising the substrate-binding cavity of obelin, only Tyr138 and His175, which are situated within the exiting helices of the loops III and IV, respectively, undergo a noticeable repositioning in response to Ca^{2+}

binding (Liu *et al.*, 2006). Since the EF-hand motifs III and IV are paired, the reorientation of the imidazole ring of His175 and Tyr138 from the internal cavity can occur simultaneously, leading to both the origin of the peroxy anion and the appearance of a water molecule at a hydrogen-bonding distance from the N1 atom instead of the hydroxyl group of Tyr138 (Fig. 8). It is noteworthy that Tyr138 returns into the cavity to practically the same position after removing calcium ions from Ca^{2+}-discharged obelin, pushing out the water molecule in the other position of the internal cavity (Deng *et al.*, 2004). As the p*K* of the amide anion is likely to be higher than that of the water molecule, it might be the driving force that initiates proton transfer from solvent through the 'proton channel' formed by water molecules W_2 and W_3, His64, Ser47, Asp48 and Gln65 (Fig. 9). The arrangement of a 'proton channel' connecting the internal cavity to the surface is identical both in Ca^{2+}-discharged Y138F and WT obelins.

Thus, the crystal structures of the Y138F obelin mutant in two conformational states provide further insight into the molecular mechanism of the bioluminescence reaction of Ca^{2+}-regulated photoproteins and the function of the cavity-forming amino-acid residues in this process. Although obelin differs from other hydromedusan Ca^{2+}-regulated photoproteins in some properties (bioluminescence spectrum, kinetics *etc.*), they are suggested to have a common bioluminescence mechanism.

We acknowledge the use of beamline BL17U1 at the Shanghai Synchrotron Radiation Facility, China. This work was supported by RFBR grants 12-04-91153, 12-04-00131 and the China–Russia International Collaboration grant from the Chinese Academy of Sciences and NSFC, by the Programs of the Government of the Russian Federation 'Measures to Attract Leading Scientists to Russian Educational Institutions' (grant 11.G34.31.0058) and 'Molecular and Cellular Biology' of the RAS, the President of the Russian Federation 'Leading Science School' (grant 3951.2012.4). PVN and EVE were supported by RFBR grant 14-04-31092.

References

Adams, P. D. *et al.* (2010). *Acta Cryst.* D**66**, 213–221.
Adams, P. D., Grosse-Kunstleve, R. W., Hung, L.-W., Ioerger, T. R., McCoy, A. J., Moriarty, N. W., Read, R. J., Sacchettini, J. C., Sauter, N. K. & Terwilliger, T. C. (2002). *Acta Cryst.* D**58**, 1948–1954.
Aghamaali, M. R., Jafarian, V., Sariri, R., Molakarimi, M., Rasti, B., Taghdir, M., Sajedi, R. H. & Hosseinkhani, S. (2011). *Protein J.* **30**, 566–574.
Allen, D. G., Blinks, J. R. & Prendergast, F. G. (1977). *Science*, **195**, 996–998.
Alvarez, J. & Montero, M. (2002). *Cell Calcium*, **32**, 251–260.
Berman, H. M., Westbrook, J., Feng, Z., Gilliland, G., Bhat, T. N., Weissig, H., Shindyalov, I. N. & Bourne, P. E. (2000). *Nucleic Acids Res.* **28**, 235–242.
Blinks, J. R., Wier, W. G., Hess, P. & Prendergast, F. G. (1982). *Prog. Biophys. Mol. Biol.* **40**, 1–114.
Cormier, M. J., Hori, K., Karkhanis, Y. D., Anderson, J. M., Wampler, J. E., Morin, J. G. & Hastings, J. W. (1973). *J. Cell. Physiol.* **81**, 291–297.
Deng, L., Markova, S. V., Vysotski, E. S., Liu, Z.-J., Lee, J., Rose, J. & Wang, B.-C. (2004). *J. Biol. Chem.* **279**, 33647–33652.
Deng, L., Vysotski, E. S., Liu, Z.-J., Markova, S. V., Malikova, N. P., Lee, J., Rose, J. & Wang, B.-C. (2001). *FEBS Lett.* **506**, 281–285.
Deng, L., Vysotski, E. S., Markova, S. V., Liu, Z.-J., Lee, J., Rose, J. & Wang, B.-C. (2005). *Protein Sci.* **14**, 663–675.
Eglen, R. M. & Reisine, T. (2008). *Assay Drug Dev. Technol.* **6**, 659–671.
Emsley, P. & Cowtan, K. (2004). *Acta Cryst.* D**60**, 2126–2132.
Eremeeva, E. V., Markova, S. V., Frank, L. A., Visser, A. J., van Berkel, W. J. & Vysotski, E. S. (2013). *Photochem. Photobiol. Sci.* **12**, 1016–1024.
Eremeeva, E. V., Markova, S. V., van Berkel, W. J. & Vysotski, E. S. (2013). *J. Photochem. Photobiol. B*, **127**, 133–139.
Eremeeva, E. V., Natashin, P. V., Song, L., Zhou, Y., van Berkel, W. J., Liu, Z.-J. & Vysotski, E. S. (2013). *Chembiochem*, **14**, 739–745.
Fagan, T. F., Ohmiya, Y., Blinks, J. R., Inouye, S. & Tsuji, F. I. (1993). *FEBS Lett.* **333**, 301–305.
Frank, L. A., Borisova, V. V., Markova, S. V., Malikova, N. P., Stepanyuk, G. A. & Vysotski, E. S. (2008). *Anal. Bioanal. Chem.* **391**, 2891–2896.
Grienberger, C. & Konnerth, A. (2012). *Neuron*, **73**, 862–885.
Hastings, J. W. & Gibson, Q. H. (1963). *J. Biol. Chem.* **238**, 2537–2554.
Hastings, J. W., Mitchell, G., Mattingly, P. H., Blinks, J. R. & Van Leeuwen, M. (1969). *Nature (London)*, **222**, 1047–1050.
Head, J. F., Inouye, S., Teranishi, K. & Shimomura, O. (2000). *Nature (London)*, **405**, 372–376.
Hori, K., Wampler, J. E., Matthews, J. C. & Cormier, M. J. (1973). *Biochemistry*, **12**, 4463–4468.
Illarionov, B. A., Bondar, V. S., Illarionova, V. A. & Vysotski, E. S. (1995). *Gene*, **153**, 273–274.
Illarionov, B. A., Frank, L. A., Illarionova, V. A., Bondar, V. S., Vysotski, E. S. & Blinks, J. R. (2000). *Methods Enzymol.* **305**, 223–249.
Illarionov, B. A., Markova, S. V., Bondar, V. S., Vysotski, E. S. & Gitelzon, I. I. (1992). *Dokl. Akad. Nauk*, **326**, 911–913.
Inouye, S. (2008). *J. Biochem.* **143**, 711–717.
Inouye, S., Noguchi, M., Sakaki, Y., Takagi, Y., Miyata, T., Iwanaga, S., Miyata, T. & Tsuji, F. I. (1985). *Proc. Natl Acad. Sci. USA*, **82**, 3154–3158.
Inouye, S. & Tsuji, F. I. (1993). *FEBS Lett.* **315**, 343–346.
Lee, J., Glushka, J. N., Markova, S. V. & Vysotski, E. S. (2001). *Bioluminescence and Chemiluminescence 2000*, edited by J. F. Case, P. J. Herring, B. H. Robison, S. H. D. Haddock, L. J. Kricka & P. E. Stanley, pp. 92–102. Singapore: World Scientific.
Liu, Z.-J., Stepanyuk, G. A., Vysotski, E. S., Lee, J., Markova, S. V., Malikova, N. P. & Wang, B.-C. (2006). *Proc. Natl Acad. Sci. USA*, **103**, 2570–2575.
Liu, Z.-J., Vysotski, E. S., Chen, C.-J., Rose, J. P., Lee, J. & Wang, B.-C. (2000). *Protein Sci.* **9**, 2085–2093.
Liu, Z.-J., Vysotski, E. S., Deng, L., Lee, J., Rose, J. & Wang, B.-C. (2003). *Biochem. Biophys. Res. Commun.* **311**, 433–439.
Malikova, N. P., Stepanyuk, G. A., Frank, L. A., Markova, S. V., Vysotski, E. S. & Lee, J. (2003). *FEBS Lett.* **554**, 184–188.
Markova, S. V., Burakova, L. P., Frank, L. A., Golz, S., Korostileva, K. A. & Vysotski, E. S. (2010). *Photochem. Photobiol. Sci.* **9**, 757–765.
Markova, S. V., Burakova, L. P., Golz, S., Malikova, N. P., Frank, L. A. & Vysotski, E. S. (2012). *FEBS J.* **279**, 856–870.
Markova, S. V., Vysotski, E. S., Blinks, J. R., Burakova, L. P., Wang, B.-C. & Lee, J. (2002). *Biochemistry*, **41**, 2227–2236.
Markova, S. V., Vysotski, E. S. & Lee, J. (2001). *Bioluminescence and Chemiluminescence 2000*, edited by J. F. Case, P. J. Herring, B. H. Robison, S. H. D. Haddock, L. J. Kricka & P. E. Stanley, pp. 115–118. Singapore: World Scientific.
McCapra, F. & Chang, Y. C. (1967). *Chem. Commun.*, pp. 1011–1012.
McCoy, A. J., Grosse-Kunstleve, R. W., Adams, P. D., Winn, M. D., Storoni, L. C. & Read, R. J. (2007). *J. Appl. Cryst.* **40**, 658–674.

Morin, J. G. (1974). *Coelenterate Biology: Reviews and New Perspectives*, edited by L. Muscatine & H. M. Lenhoff, pp. 397–438. New York: Academic Press.
Murshudov, G. N., Skubák, P., Lebedev, A. A., Pannu, N. S., Steiner, R. A., Nicholls, R. A., Winn, M. D., Long, F. & Vagin, A. A. (2011). *Acta Cryst.* D**67**, 355–367.
Musicki, B., Kishi, Y. & Shimomura, O. (1986). *J. Chem. Soc. Chem. Commun.*, pp. 1566–1568.
Nelson, M. R. & Chazin, W. J. (1998). *Biometals*, **11**, 297–318.
Ohmiya, Y., Ohashi, M. & Tsuji, F. I. (1992). *FEBS Lett.* **301**, 197–201.
Ohmiya, Y. & Tsuji, F. I. (1993). *FEBS Lett.* **320**, 267–270.
Oort, B. van, Eremeeva, E. V., Koehorst, R. B., Laptenok, S. P., van Amerongen, H., van Berkel, W. J., Malikova, N. P., Markova, S. V., Vysotski, E. S., Visser, A. J. & Lee, J. (2009). *Biochemistry*, **48**, 10486–10491.
Otwinowski, Z. & Minor, W. (1997). *Methods Enzymol.* **276**, 307–326.
Powers, M. L., McDermott, A. G., Shaner, N. C. & Haddock, S. H. (2013). *Biochem. Biophys. Res. Commun.* **431**, 360–366.
Pozzan, T. & Rudolf, R. (2009). *Biochim. Biophys. Acta*, **1787**, 1317–1323.
Prasher, D., McCann, R. O. & Cormier, M. J. (1985). *Biochem. Biophys. Res. Commun.* **126**, 1259–1268.
Prasher, D. C., McCann, R. O., Longiaru, M. & Cormier, M. J. (1987). *Biochemistry*, **26**, 1326–1332.
Roura, S., Gálvez-Montón, C. & Bayes-Genis, A. (2013). *J. Cell. Mol. Med.* **17**, 693–703.
Schnitzler, C. E., Pang, K., Powers, M. L., Reitzel, A. M., Ryan, J. F., Simmons, D., Tada, T., Park, M., Gupta, J., Brooks, S. Y., Blakesley, R. W., Yokoyama, S., Haddock, S. H., Martindale, M. Q. & Baxevanis, A. D. (2012). *BMC Biol.* **10**, 107.
Shimomura, O. & Johnson, F. H. (1972). *Biochemistry*, **11**, 1602–1608.
Shimomura, O. & Johnson, F. H. (1975). *Nature (London)*, **256**, 236–238.
Shimomura, O., Johnson, F. H. & Saiga, Y. (1962). *J. Cell. Comp. Physiol.* **59**, 223–239.
Stepanyuk, G. A., Golz, S., Markova, S. V., Frank, L. A., Lee, J. & Vysotski, E. S. (2005). *FEBS Lett.* **579**, 1008–1014.
Teranishi, K., Ueda, K., Hisamatsu, M. & Yamada, T. (1995). *Biosci. Biotechnol. Biochem.* **59**, 104–107.
Teranishi, K., Ueda, K., Nakao, H., Hisamatsu, M. & Yamada, T. (1994). *Tetrahedron Lett.* **35**, 8181–8184.
Titushin, M. S., Feng, Y., Stepanyuk, G. A., Li, Y., Markova, S. V., Golz, S., Wang, B.-C., Lee, J., Wang, J., Vysotski, E. S. & Liu, Z.-J. (2010). *J. Biol. Chem.* **285**, 40891–40900.
Tomilin, F. N., Antipina, L. Y., Vysotski, E. S., Ovchinnikov, S. G. & Gitelzon, I. I. (2008). *Dokl. Biochem. Biophys.* **422**, 279–284.
Tsuji, F. I., Ohmiya, Y., Fagan, T. F., Toh, H. & Inouye, S. (1995). *Photochem. Photobiol.* **62**, 657–661.
Usami, K. & Isobe, M. (1996). *Tetrahedron*, **52**, 12061–12090.
Vysotski, E. S. & Lee, J. (2004). *Acc. Chem. Res.* **37**, 405–415.
Vysotski, E. S. & Lee, J. (2007). *Luciferases and Fluorescent Proteins: Principles and Advances in Biotechnology and Bioimaging*, edited by V. R. Viviani & Y. Ohmiya, pp. 19–41. Kerala: Transworld Research Network.
Vysotski, E. S., Liu, Z.-J., Markova, S. V., Blinks, J. R., Deng, L., Frank, L. A., Herko, M., Malikova, N. P., Rose, J. P., Wang, B.-C. & Lee, J. (2003). *Biochemistry*, **42**, 6013–6024.
Vysotski, E. S., Liu, Z.-J., Rose, J., Wang, B. C. & Lee, J. (1999). *Acta Cryst.* D**55**, 1965–1966.
Vysotski, E. S., Liu, Z.-J., Rose, J., Wang, B. C. & Lee, J. (2001). *Acta Cryst.* D**57**, 1919–1921.
Vysotski, E. S., Markova, S. V. & Frank, L. A. (2006). *Mol. Biol.* **40**, 355–367.
Winn, M. D. *et al.* (2011). *Acta Cryst.* D**67**, 235–242.